NAVAL POSTGRADUATE SCHOOL
Monterey, California

THESIS

FUSION NEUTRON DAMAGE TO A CHARGE COUPLED DEVICE CAMERA

by

Christopher Dean Amaden

September, 1997

Thesis Advisor: William B. Maier II
Co-Advisor: Xavier K. Maruyama

REPORT DOCUMENTATION PAGE

Form Approved OMB No. 0704-0188

1. AGENCY USE ONLY *(Leave blank)*	2. REPORT DATE September 1997	3. REPORT TYPE AND DATES COVERED Master's Thesis

4. FUSION NEUTRON DAMAGE TO A CHARGE COUPLED DEVICE CAMERA

5. FUNDING NUMBERS

6. AUTHOR(S)
Amaden, Christopher, D.

7. PERFORMING ORGANIZATION NAME(S) AND ADDRESS(ES)
Naval Postgraduate School
Monterey CA 93943-5000

8. PERFORMING ORGANIZATION REPORT NUMBER

9. SPONSORING/MONITORING AGENCY NAME(S) AND ADDRESS(ES)

10. SPONSORING/MONITORING AGENCY REPORT NUMBER

11. SUPPLEMENTARY NOTES The views expressed in this thesis are those of the author and do not reflect the official policy or position of the Department of Defense or the U.S. Government.

12a. DISTRIBUTION/AVAILABILITY STATEMENT
Approved for public release; distribution is unlimited.

12b DISTRIBUTION CODE

13. ABSTRACT

A charge coupled device (CCD) camera's performance has been degraded by damage produced by 14 MeV neutrons (n) from the Rotating Target Neutron Source. High-energy neutrons produce atomic dislocation in doped silicon electronics. This thesis explores changes in Dark Current (J), Charge Transfer Inefficiency (CTI), and Contrast Transfer Function (CTF) as measures of neutron damage.

The camera was irradiated to a fluence, ϕ, of 6.60×10^{12} n/cm^2. The camera temperature was lowered from room temperature to 267 K at a fluence of 4.7×10^{11} n/cm^2 to preclude saturation of the camera picture. With temperature compensations, J increased linearly with ϕ. Four data points for J, CTF (ideal of 1.0), and CTI (ideal of 0.0) are:

Fluence (n/cm^2)	0	4.7×10^{11}	4.7×10^{11}	6.60×10^{12}
Temp (K)	292.1	296.1	267	266.8
J (nA/cm^2)	0.37	11	0.93	9.8
CTF	0.89	0.37	0.82	0.48
CTI	1.3×10^{-4}	1.2×10^{-3}	2.4×10^{-4}	1.6×10^{-3}

Neutron irradiation significantly degraded the CCD camera performance; however, operating the camera at lower temperatures significantly reduces the effects. Damage thresholds for fluences greater than 6.60×10^{12} n/cm^2 and for all temperatures can be extrapolated from the results of this work.

14. SUBJECT TERMS: Neutron Radiation, Charge Coupled Device, Dark Current, Contrast Transfer Function, Charge Transfer Inefficiency.	15. NUMBER OF PAGES 53
	16 PRICE CODE

17. SECURITY CLASSIFICATION OF REPORT	18. SECURITY CLASSIFICATION OF THIS PAGE	19. SECURITY CLASSIFICATION OF ABSTRACT	20 LIMITATION OF ABSTRACT
Unclassified	Unclassified	Unclassified	UL

NSN 7540-01-280-5500

Standard Form 298 (Rev. 2-89)

Prescribed by ANSI Std 239-18 298-102

Approved for public release; distribution is unlimited.

FUSION NEUTRON DAMAGE TO A CHARGE COUPLED DEVICE CAMERA

Christopher D. Amaden
Lieutenant, United States Navy
B. S., University of South Florida, 1990

Submitted in partial fulfillment
of the requirements for the degree of

MASTER OF SCIENCE IN PHYSICS

from the

NAVAL POSTGRADUATE SCHOOL
September 1997

ABSTRACT

A charge coupled device (CCD) camera's performance has been degraded by damage produced by 14 MeV neutrons (n) from the Rotating Target Neutron Source. High-energy neutrons produce atomic dislocation in doped silicon electronics. This thesis explores changes in Dark Current (J), Charge Transfer Inefficiency (CTI), and Contrast Transfer Function (CTF) as measures of neutron damage.

The camera was irradiated to a fluence, ϕ, of 6.60×10^{12} n/cm^2. The camera temperature was lowered from room temperature to 267 K at a fluence of 4.7×10^{11} n/cm^2 to preclude saturation of the camera picture. With temperature compensations, J increased linearly with ϕ. Four data points for J, CTF (ideal of 1.0) and CTI (ideal of 0) are:

Fluence (n/cm^2)	0	4.7×10^{11}	4.7×10^{11}	6.60×10^{12}
Temp (K)	292.1	296.1	267	266.8
J (nA/cm^2)	0.37	11	0.93	9.8
CTF	0.89	0.37	0.82	0.48
CTI	1.3×10^{-4}	1.2×10^{-3}	2.4×10^{-4}	1.6×10^{-3}

Neutron irradiation significantly degraded CCD camera performance; however, operating the camera at lower temperatures significantly reduces the effects. Damage thresholds for fluences greater than 6.60×10^{12} n/cm^2 and for all temperatures can be extrapolated from the results of this work.

TABLE OF CONTENTS

LIST OF SYMBOLS

A	Area of a pixel
b	Digital bias offset
c_e	Charge transfer efficiency
c	Combined damage coefficient
C	Capacitance of the CMOS
C_B	Capacitance of the bulk scr region
C_0	Capacitance of the oxide layer
C_N	Capacitance of the inversion layer
D_{it}	Interface state density
e	Number of electrons
E_f	Electric field magnitude
E	Effective half gap energy
E_F	Fermi energy
E_G	Gap energy
G	Steady state generation rate per unit volume
G_s	Steady state scr interface generate rate per unit area
h	Planck's constant
j	Row number
J	Dark current
J_0	Temperature independent dark current
J_s	Surface dark current
k	Boltzmann's constant
K	Surface generation damage coefficient
K_g	Generation damage coefficient
K_o	Oxide dielectric constant
K_s	Semiconductor dielectric constant
n	Total number of rows
n_e	Electron concentration
n_i	Intrinsic carrier concentration
n_z	Number of zeros during CCD clocking
N_D	Donor doping concentration
m_e	Mass of an electron

m_h Mass of a hole

p Hole concentration

P Number of CCD clocking phases

q Magnitude of electronic charge

Q_{bias} Charge due to bias

Q_{sig} Charge due to signal

R_j Average digital value of the j^{th} row of pixels

s Surface generation velocity

s_0 Pre-irradiated surface generation velocity

t_e Exposure time

t_r Readout time

T Temperature

T_0 Reference temperature

V_G Gate voltage

V_r Reference voltage

x_d Depletion width

x_o Oxide width

η Charge transfer inefficiency

ε_o Permitivity of free space

ϕ Neutron fluence

φ Electrostatic potential

φ_F Fermi potential

φ_s Electrostatic potential at the SiO-substrate interface

μ Mean value

ρ Charge density

σ Standard deviation

τ_g Generation lifetime

τ_{g0} Pre-irradiated generation lifetime

ACKNOWLEDGEMENT

The author would like to acknowledge the financial support provided by Lawrence Livermore National Laboratories.

The author wants to thank Mr. Craig Sangster of Lawrence Livermore National Laboratories for his expertise and guidance; Prof. Edward Morse and Mr. Anthony Belian, both of University of California, Berkeley for their direct support of the experiment; and Prof. William Maier, Prof. Xavier Maruyama, and Prof. James Luscombe of the Naval Postgraduate School for their guidance.

I. INTRODUCTION

Lawrence Livermore National Laboratory (LLNL) has been designated as the site of the National Ignition Facility (NIF). The purpose of NIF is to maintain nuclear stockpile verification by without underground nuclear tests. Stockpile verification is done partly by igniting fuel pellets composed of deuterium and tritium.

One challenge for NIF is to monitor these contained thermonuclear fusion reactions. The deuterium-tritium (DT) reaction yields approximately 17 MeV of kinetic energy; 14 MeV leaves with the neutron and 3 MeV remains with the alpha particle.

$$D + T \rightarrow \alpha + n + 17MeV$$

14 MeV neutrons will interact with the diagnostic equipment used to monitor the reaction and other conditions in the reaction chamber and thus may interfere with the monitoring of the reaction. LLNL is considering several engineering solutions to the problem of the adverse radiation environment at NIF.

One key diagnostic component is the Charge Coupled Device (CCD) camera, used extensively in NOVA and other current fusion studies facilities. The purpose of this research is to determine the damage and performance degradation of a CCD camera irradiated by 14 MeV neutrons.

II. PHYSICS OF THE EXPERIMENT

A. CHARGE COUPLED DEVICE THEORY

CCD's are composed of CMOS (complementary metal oxide semiconductor) devices arranged in arrays. The theory of CCD operation can be largely explained through the operation of CMOS. We will explain the pertinent aspects of CMOS theory. Except where noted, the theory used was developed in Modular Series on Solid State Devices, Advanced MOS Devices [Ref. 1].

1. Complementary Metal Oxide Semiconductor Theory

a) Ideal Structure

Individual CMOS are constructed in layers, see Figure 1. The top layer is a metal plate followed by a thin (0.01-1.0μm) SiO_2 layer, and then a doped silicon substrate. On the bottom is another metal plate to provide electrical connection to the substrate. The top metal layer is called the gate.

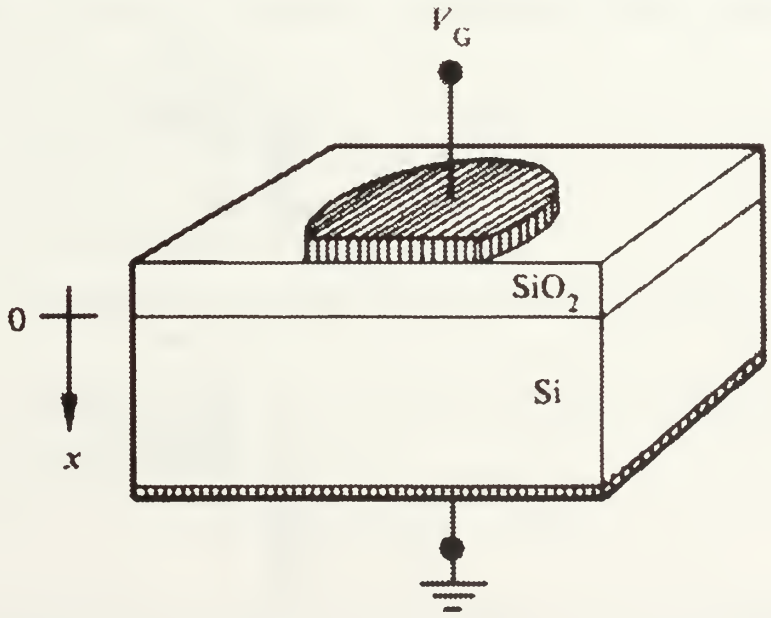

Figure 1. CMOS structure. From Ref. [11]

There are essentially three biases to consider. Figure 2 shows the charge block diagrams, where M, O, and S are for metal, oxide, and semiconductor. For n type CMOS (p type yield the same result for opposite polarities), a positive applied voltage will cause an accumulation of negative charge at the interface between the substrate and the SiO_2 layer. This configuration is called *Accumulation*. Because there are excess electrons in the n type CMOS, there are always sufficient electrons available to accumulate at the interface.

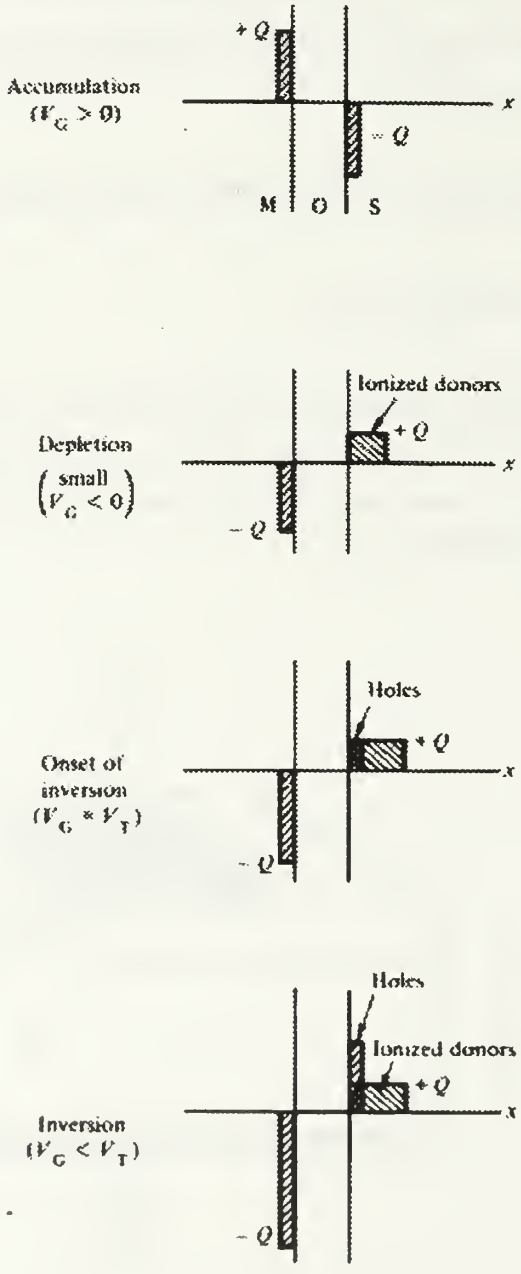

Figure 2. CMOS biases for n type semiconductor. Q is the charge. After Ref. [11]

Applying a slightly negative voltage to the gate causes the electrons to repel from the interface and leave behind a region in the substrate with a lower concentration of the extra doped electrons. This configuration is called *Depletion.*

As more negative voltage is applied, the depleted region grows very little in size, but instead, more of the doped electrons are repelled from the depletion region. To balance the charge in a fixed depletion volume, the repelled electrons can be thought of as holes accumulating at the interface equal in magnitude to the applied charge. Once the hole concentration at the interface has reached the donor concentration of the doped silicon, the surface potential is then twice the Fermi potential (the Fermi potential is the level at which the highest states in a semiconductor are filled at T=0 K, which is at midgap for an idealized semiconductor and shifts up or down due to doping [Ref. 2]). This configuration (with a fixed depletion region but accumulated holes) is called Inversion or *Deep Depletion.*

After a short transition period, the CMOS is in steady state for an applied voltage. With no current flow, we can exactly solve the CMOS's state; however, the solution to the differential equations describing the electrostatic potential can not be written in closed form. For the purposes of our problem, a very close approximation is solved instead. This solution will provide us the depletion width and an idealized solution to visualize the electric field and electrostatic potential within the CMOS.

When considering an applied voltage, we invoke Poisson's equation for a first order solution to the depletion configuration, with the simplifying assumptions which lead to linear differential equations:

i) the CMOS is in steady state

ii) the metal gate is sufficiently thick that it can be considered equipotential

iii) the oxide is a perfect insulator

iv) the semiconductor is uniformly doped

v) the substrate is sufficiently thick that there will always exist a field free region

vi) the CMOS is viewed as a one dimensional device, with x is the distance from the interface of the oxide.

Poisson's equation,

$$\nabla^2 \varphi = -\frac{\rho}{\varepsilon_o} \tag{1}$$

where φ is the electrostatic potential, ρ is the charge density, and ε_0 is the permitivity of free space (see the List of Symbols), can then be applied in each of the three layers. In the metal plate, the potential is the applied potential. In the oxide layer, the charge density is

zero and so the potential is a linear function depending only on the potential on the metal plate and the potential at the interface.

For the substrate and considering our assumptions, Poisson's equation reduces to:

$$\frac{d^2}{dx^2}\varphi(x) = -\frac{\rho}{K_s \varepsilon_o}$$

where K_s is the semiconductor dielectric constant; see Figure 1 for spatial orientation. Integrating once, with ρ constant, we obtain

$$\frac{d}{dx}\varphi(x) = -\frac{\rho}{K_s \varepsilon_o} x + C \tag{2}$$

where C is a constant of integration.

The electric field is the negative gradient of the electrostatic potential. Assumption v implies that there is a region at the end of the substrate in which the electric field is zero. The width from the interface to the beginning of the zero electric field is called the depletion width, x_d. Substituting this into Equation 2 solves for our constant of integration. For $x < x_d$

$$\frac{d}{dx}\varphi(x) = \frac{\rho}{K_s \varepsilon_o}(x_d - x)$$

and is zero elsewhere. Therefore, the electric field magnitude, E_f, is:

$$E_f(x) = \frac{-\rho}{K_s \varepsilon_o}(x_d - x) \qquad 0 < x < x_d$$

$$E_f(x) = 0 \qquad x_d < x$$

Integrating again and using a potential of zero at x_d, we obtain:

$$\varphi(x) = \frac{-\rho}{2K_s \varepsilon_o}(x_d - x)^2$$

Denoting the potential at the interface, φ_s, we can solve for x_d:

$$x_d = \left(-\frac{2K_s \varepsilon_o}{\rho}\varphi_s\right)^{1/2} \tag{3}$$

For deep depletion, the region for $x < x_d$, all of the doped charges have been repelled leaving a region known as the space charge region (scr). This divides the CMOS into scr and zero electric field regions. The scr, with all of the holes accumulated at the interface, can then be approximated as intrinsic silicon. Since the scr has lost these donor electrons, the scr has a charge density of:

$$\rho = qN_D$$

where q is the magnitude of the electronic charge and N_D is the donor doping concentration.

Since the CMOS is operated in deep depletion, the surface potential is twice the Fermi potential, φ_F:

$$\varphi_s = 2\varphi_F$$

Substituting these two equations into Equation 3, we obtain:

$$x_d = \left(\frac{4K_s\varepsilon_o}{qN_D}\varphi_F\right)^{1/2}$$

b) Capacitance

A CMOS in deep depletion acts like a capacitor. This capacitance is broken down into the capacitance of the oxide, C_0, in series with that of the semiconductor. The semiconductor can be modeled as two capacitors in parallel, the capacitance, C_N, of the inversion layer and that of a maximum inversion depletion region, C_B; see Figure 3. This is expressed as:

$$C = 1/[(1/C_0) + 1/(C_B + C_N)]$$

This equation can be directly related to the material properties of the CMOS and the applied gate voltage. For the deep depletion CMOS with an applied gate voltage, the capacitance is [Ref. 1]:

$$C = \frac{C_0}{\sqrt{1 + \frac{V_G}{V_r}}}$$

where the reference voltage, V_r, is:

$$V_r = -\frac{q}{2}\frac{K_s x_o^2}{K_o^2 \varepsilon_0} N_D$$

and where N_D is the donor doping concentration, K_0 is the oxide dielectric constant, and x_o is the oxide depth.

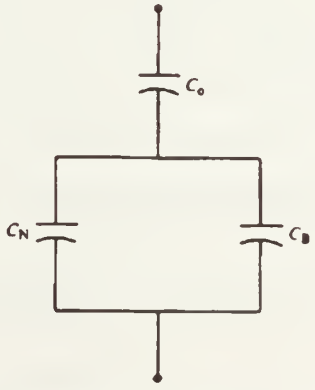

Figure 3. Effective CMOS capacitance. From Ref. [1]

These equations establish the fundamental usefulness of CMOS for CCD's. As capacitive devices, CMOS act as small charge storage devices dependent on construction and gate voltage.

c) Dark Current

The scr region can be approximated as an intrinsic semiconductor. At absolute zero, all electrons are restricted to the valence band. As the temperature increases, the electrons are thermally excited and can "jump" the gap to the conduction band and leave a hole behind. Electron-hole pairs of this type will be referred to as *Thermal EHP's*, or simply EHP's. These electrons obey Fermi statistics; thus, electron concentration in the conduction band can be calculated. With electron concentration known, the associated conductivity can be determined.

The number of electrons per unit volume in the conduction band can be found by integrating the product of the state density and the Fermi energy distribution through the conduction band to obtain the well-known result [Ref. 3]:

$$n_e = 2(2\pi m_e kT / h^2)^{3/2} e^{(E_F - E_G)/kT}$$

where n_e is electron concentration, m_e is the electron mass, k is Boltzmann's constant, T is temperature, h is Planck's constant, and E_G is the gap energy. By considering energies close to the Fermi energy compared to kT, the hole concentration, p, is [Ref. 3]

$$p = 2(2\pi m_h kT / h^2)^{3/2} e^{-E_F/kT}$$

where m_h is the hole mass. Since the number of holes is equal to the number of electrons in intrinsic semiconductors, by taking the square root of the product of n and p (eliminating the Fermi energy), one obtains the so-called intrinsic concentration, n_i, [Ref. 3]:

$$n_i = 2(2\pi kT / h^2)^{3/2} (m_e m_h)^{3/4} e^{-E_G/2kT}$$

Although our first order assumptions, i- iv above, utilized a steady state solution for CMOS parameters, the deep depletion CMOS operates in quasi-equilibrium. For a particular temperature, electrons are flowing from the valence band to the conduction band where they are available for current flow. Consider a steady state generation time, τ_g, for EHP's. Because the CMOS is operated in reverse bias, generation of EHP's greatly outweighs recombination. The generation rate per unit volume, G, is due to the number of EHP's generated and τ_g, or simply [Ref 1]:

$$G = n_i / \tau_g$$

The current flow per unit area, or *Dark Current*, is the product of the generation rate of charge per unit volume, the magnitude of the charge (electron) and the average distance through which the charge flows (depletion width) [Ref 1]:

$$J = qn_i x_d / \tau_g$$

Generation-recombination centers in the interface region also cause dark current. The periodicity of the substrate is interrupted at the interface. The bridging bonds between the bulk and the oxide do not always have partners. The deficient bonds are modeled as interface states. These interface states are not well defined energy levels; instead they are closely spaced throughout the energy gap. The analysis of generation rate

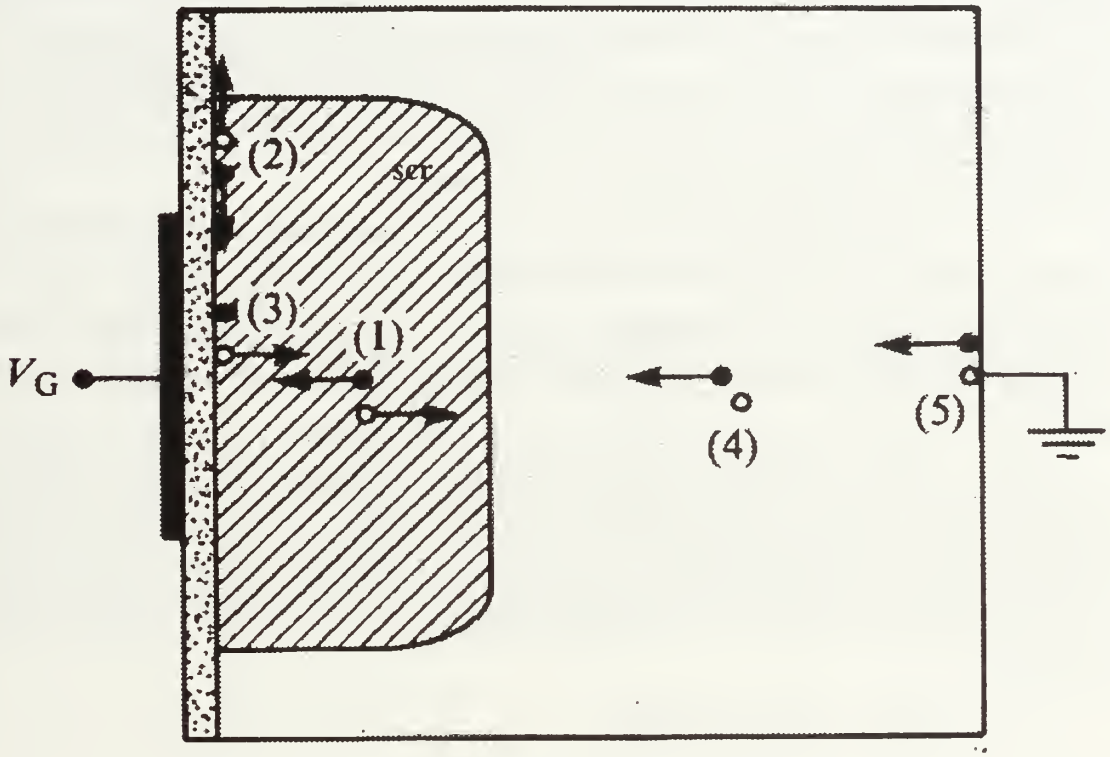

Figure 4. Dark current sources. For n-type, filled circles are holes. After Ref. [1]

is similar to that of the bulk, but the conventional approach is to consider the interface as two-dimensional and describe the phenomena at the interface in terms of a surface scr *generation velocity*, s, instead of a generation lifetime. Accordingly the surface generation rate per unit area, G_s, is given by [Ref. 1]:

$$G_s = sn_i$$

This yields an associated surface dark current, J_s, of [Ref. 1]:

$$J_s = qn_i s$$

Combining both of these sources of dark current yields:

$$J = qn_i(x_d / \tau_g + s) \tag{4}$$

Figure 4 shows five example source sites. Site 1 is within the scr, sites 2 and 3 are at the interface, site 4 is within the bulk zero electric field region and site 5 is at the substrate. Sites 1, 2, and 3 will contribute to the dark current, while sites 4 and 5 have a probability of contributing depending on their distance to the scr.

2. CCD Operation

a) Imaging

CMOS are used in CCD cameras for imaging. A gate voltage, V_G, is applied to the CMOS. When the CMOS is irradiated with photons from the visible and near infrared wavelengths, these photons generate one EHP for each absorbed photon. The minority carrier is of interest because CMOS are reverse biased. Those minority carriers generated in the scr and within one diffusion length, on average, are collected without loss to recombination; otherwise, they recombine.

The collected positive charge in the scr is proportional to the number of incident photons. This charge is therefore subtracted from the initial negative charge placed on the CMOS due to the negative gate voltage. After a sufficient integration time, the charge is transferred out to a controller where the difference in charge is attributed to light.

The technique used for readout of the CCD array is a row by row shift out. In this process, the entire array is shifted up one row, and the top row is shifted to the shift register where the charge is shifted out to the right and digitized. The entire array is then shifted up again and the process is repeated until the entire array has been read out to the controller.

b) Charge Transfer

Charge transfer from one carrier well (CMOS) to another for readout is through drift and diffusion. For CCD's, the dominant mechanism is due to drift. Charge Transfer Inefficiency (CTI) is defined as the fraction of charge remaining after a charge transfer event. A useful approximate solution for CCD's CTI is the *Charge-Control Solution*. Boer [Ref. 2] shows that the CTI can be made as low as desired with sufficiently long readout times. However, in practice, the dominant limitation for very low CTI is the effect of interface states. Interface states are continuously distributed energy states in the band gap at the semiconductor/oxide interface. They affect the CTI by capturing charge and emitting them at a slower rate than non-captured charges [Ref. 2]; Boer finds:

$$\eta = \{qkTD_{it}/(Q_{sig} + Q_{bias})\}\ln(1 + Pn_z) \tag{5}$$

where η is the CTI, n_z is the number of digital zeros following the signal, D_{it} is the interface state density, Q_{sig} and Q_{bias} are the signal and bias charges, and P is the number of

clocking cylces. By maintaining some small bias charge (fat zero) in the CCD, CTI can be improved significantly.

The applicable implications of this result are that CTI is a function of the temperature, the number of interface states, and amount of charge left in the carrier well. For a larger amount of light incident on the cell, there is lower Q_{sig} leading to a larger (worse) CTI.

B. NEUTRON RADIATION DAMAGE

1. Basic Mechanisms

There are three mechanisms of radiation damage to CCD's: *Total Ionizing Dose Effects*, *Transient Effects*, and *Displacement Damage* [Ref. 4]. This thesis primarily investigates cumulative "permanent" damaged caused by neutron irradiation. A glass protective plate covering the head of the CCD and either an aluminum plate for most of the exposures or a duct tape covering when the camera was close to the source shielded charged particles from the DT reaction. Transient effects were observed in this work during irradiation but are only superficially treated here.

2. Displacement Damage

When 14 MeV neutrons collide with the silicon atoms in the CMOS, several hundred stable defects are created in that region [Ref. 5]. These defects produce energy levels in the bandgap, but only those near midgap contribute to dark current increases [Ref. 4, 5]. As more levels are added, the generation time increases. The other significant effect neutron-silicon collisions induce is an increase in interface states [Ref. 6], which likewise leads to an increase in the surface generation velocity. Both of these parameters have been successfully modeled [Ref. 5]:

$$1/\tau_g = 1/\tau_{g0} + \phi/K_g$$

$$s = s_0 + \phi/K$$

where K_g and K are the generation and surface damage coefficients, τ_{g0} and s_0 are the pre-irradiated generation time and surface velocity. Recalling that in deep depletion the scr is treated as intrinsic silicon, these results are applied to Equation 4:

$$J = qn_i x_d[(1/\tau_g + \phi/K_g) + s + \phi/K)$$

Next we note that the temperature dominance of the dark current is due to the intrinsic carrier concentration term [Ref. 5]. It has the form of:

$$f(T) = (T/T_0)^{3/2} e^{-E/kT} \tag{6}$$

where E is the effective half gap energy. This allows us to simplify our dark current expression to:

$$J = (J_0 + c\phi) f(T) \tag{7}$$

where J_0 is the temperature independent portion of the dark current, and c is the combined damage coefficient: $c = 1/K_g + 1/K$.

III. EXPERIMENTAL SETUP

This experiment was conducted in the basement at Etcheverry Hall on the University of California, Berkeley. 14 MeV neutrons were produced by the Rotating Target Neutron Source (RTNS). We will discuss its basic arrangement. The digital camera and controller were provided by LLNL. Bechtel Nevada Laboratories provided the test bed equipment for high-resolution imaging.

A. ROTATING TARGET NEUTRON SOURCE

RTNS is a 2-5 mA deuteron accelerator with a maximum beam energy of 399 keV which impinges on a rotating, internally cooled, tritiated copper target; see Figure 5. The copper target is impregnated with approximately 110 Ci of tritium. Neutrons are produced isotropically. The maximum associated production rate of 14 MeV neutrons is 1.0×10^{12} n/sec [Ref 7].

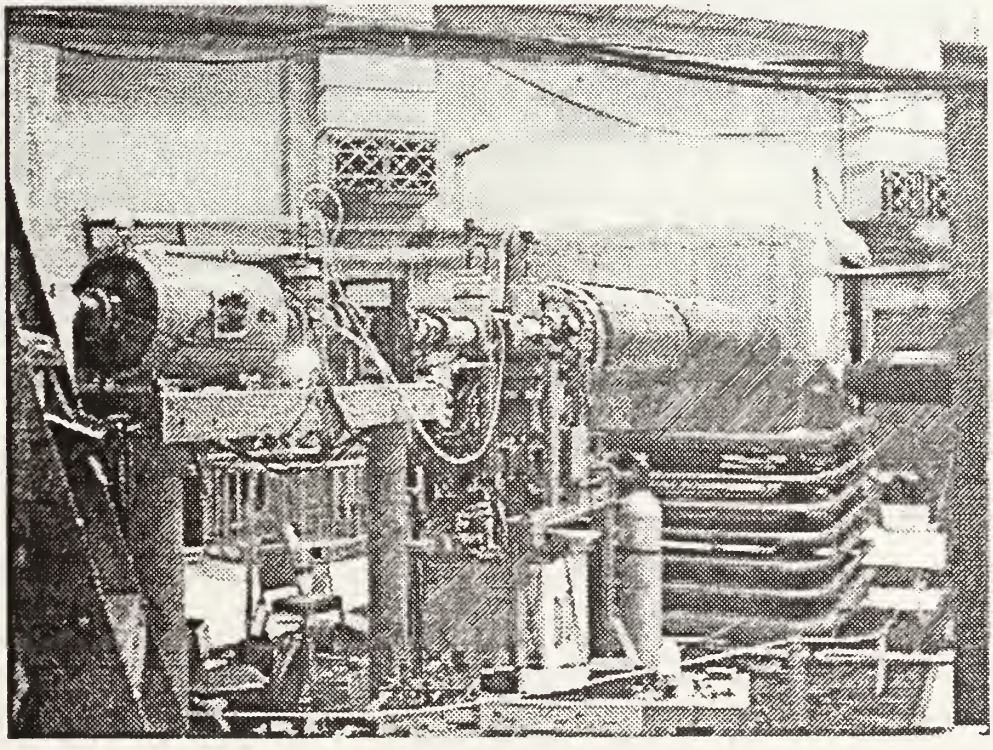

Figure 5. RTNS Accelerator Column

B. DIGITAL CAMERA AND CONTROLLER

The camera and controller together provide the means to take digital pictures. The camera head and controller used in this experiment are both manufactured by Princeton Instruments. Our camera head is then mounted for stability and connected with either fiber optics or regular cabling to the controller.

1. EEV 1152 x 1242 CCD Camera

This model is designed for large format, high pixel density pictures of high resolution. The specifications of the camera are provided in the Appendix. A heat sink is required for proper operation of this camera. It generates approximately 1 Watt of heat when operated at 250 K. This heat is dissipated via the Peltier cooler at a conversion of 16:1 in heat loss. The heat is then taken away by a coolant [Ref. 9].

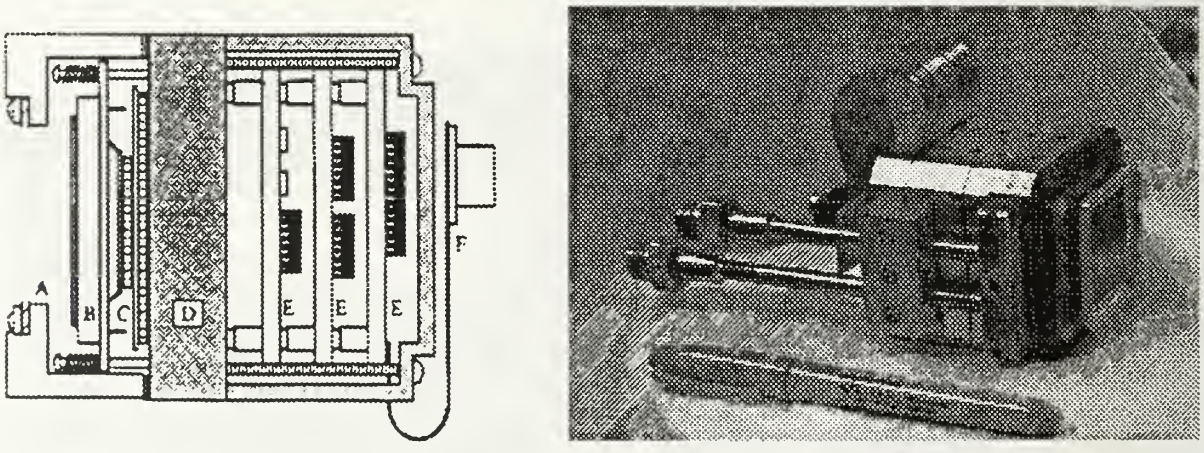

Figure 6. CCD camera schematic and photograph with glass holder removed. After Ref. [9]

The camera is shown in Figure 6. A window (A), glass removed for this experiment, lets in light for the CCD (B) to read. The CCD has a thin piece of glass covering the head. The cooler (C) generates heat exhausted via the copper heat sink (D). The flexible connector (F) is attached to the camera electronics (E) and the controller.

2. ST-138 Camera Controller

The camera controller provides dc power, clock timing, and command signals. It also provides control of the Peltier cooler. The primary electronic function of the controller is to convert the analog signal provided by the camera into digital information. By using commercial software, operation of the camera via the controller can provide a wide range of control features. This allows the operator to tailor timing, picture size, shutter usage, cooling, and other parameters to fit the prescribed use.

C. TEST BENCH

The test bench was located outside the radiation chamber on a level table. It was used prior to and after each irradiation of the camera. The test bench, camera controller, and associated computer software were used to obtain all images in this experiment.

1. Arrangement

The test bench used a 500 mm Gaertner rail, see Figure 7. At one end, a xenon flash head within an optiliner barrel provided a plane source of white light, the structure to hold the filters, and a lens for focusing. This light passed through a 530 nm bandpass filter through ND filters, and finally through either a resolution image slide (see Figure 7) or a blank slide. The next stage was the lens to focus the image or light onto the final component, the CCD camera. The camera was bolted to a locking rail slide and scissors jack for height and length fine adjustments. Cardboard tubing and black cloth blocked out external light during bench test.

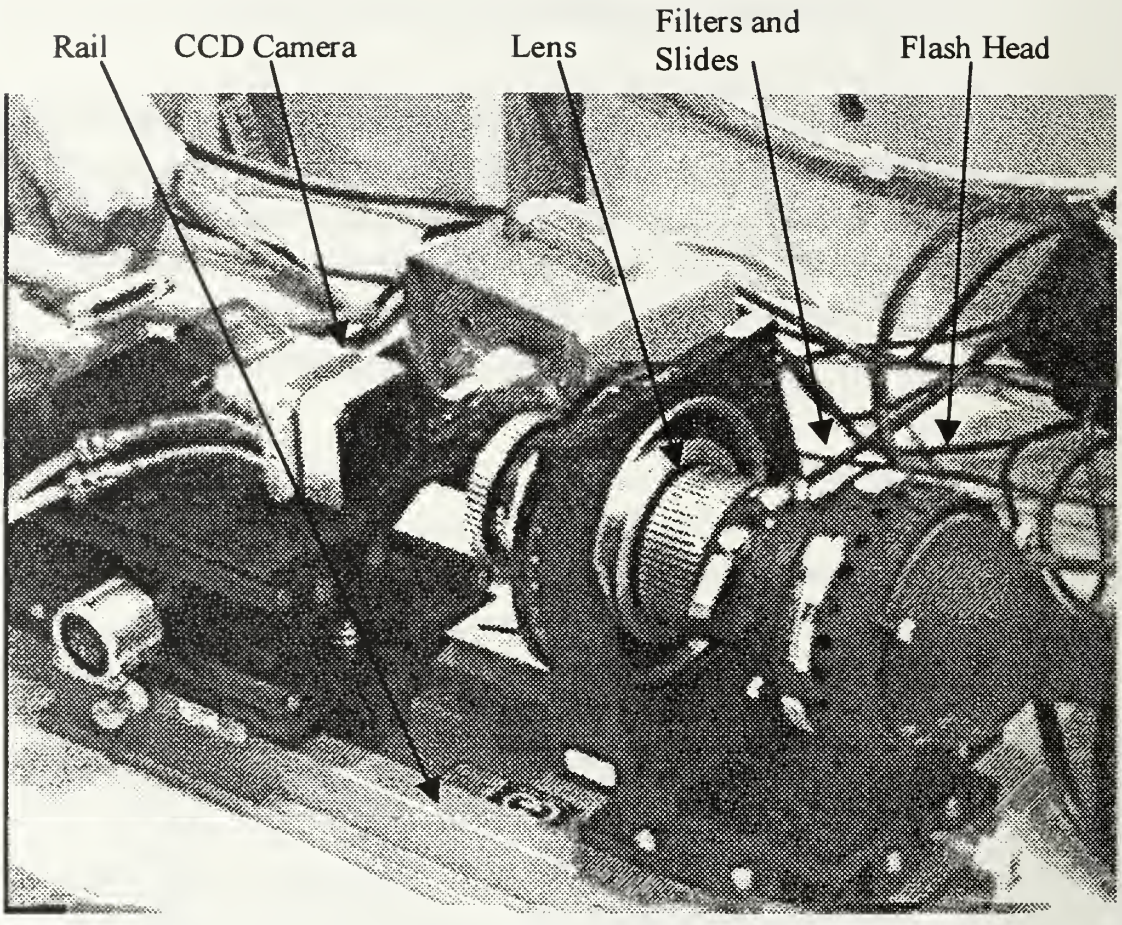

Figure 7. Test bench setup

For the experiment, the camera was removed from the test bench, irradiated in the radiation chamber, and then replaced on the test bench. The physical removal and replacement meant that focusing of the camera was required for each set of images. This was accomplished by mounting the camera on the locking rail slide with visual alignment. We used the controller in conjunction with computer software to take a picture of the image and then manually adjusted the scissors jack and rail slide, repeating this process until the image, see Figure 8, was in focus and properly centered. Thus, images were not projected on identical pixels in different runs.

D. EXPERIMENTAL PROCEDURE

The experiment was conducted over ten days. The basic procedure remained the same, but some modifications were made, as the camera damage became more apparent.

1. Basic Procedure

a) Transfer Procedures

After a set of test bench pictures was taken, all of the test bench equipment was turned off (controller, xenon flash lamp, and pump). A staging area at the opening of the radiation chamber was established, and the controller, camera, pump, and all of the associated tubing and cabling were transferred to this area. A wooden ladder was used as the portable camera mount within the radiation chamber. It was placed to provide the correct distance from the neutron source to the camera, depending on the amount of neutron irradiation desired for the shot. The camera was then mounted on the ladder and the support equipment attached. In the radiation chamber, a specially designed periscope mount was attached to the face of the camera to provide a uniform light source for monitoring camera operation during irradiation.

Table 1.

Fluence Timeline and Bench #

Bench Number	Date Time March 1997	Fluence n/cm^2	Bench #	Date Time March 1997	Fluence n/cm^2
1	13 11:45	0	17	17 10:27	1.00E+09
2	13 15:23	3.80E+04	18	17 13:23	3.00E+09
3	13 16:43	1.80E+06	19	17 15:35	8.10E+09
4	14 09:05	1.80E+06	20	17 17:23	1.70E+10
5	14 10:38	5.10E+06	21	18 08:42	1.70E+10
6	14 14:41	9.80E+06	22	18 11:18	3.70E+10
7	14 16:01	2.00E+07	23	18 13:42	6.10E+10
8	14 17:09	3.30E+07	24	18 20:31	1.10E+11
9	15 09:28	3.30E+07	25	19 09:05	1.10E+11
10	15 10:21	3.30E+07	26	20 09:47	2.90E+11
11	15 11:45	5.10E+07	27	20 14:04	4.70E+11
12	15 14:16	9.00E+07	28	20 15:22	5.13E+11
13	15 15:55	2.20E+08	29	21 09:41	3.10E+12
14	15 17:11	5.00E+08	30	24 08:48	6.60E+12
15	16 15:25	5.00E+08	31	24 08:52	6.60E+12
16	17 08:25	5.00E+08			

After the camera was irradiated by neutrons, an adequate amount of time was allowed for the radiation level in the chamber to fall to acceptable levels; toward the end of the experiment, this meant overnight. The chamber was then opened, the equipment secured, a radiological transfer area established, and the camera and associated

equipment were transferred back to the test bench where the camera was refocused and aligned. At that point, a series of test bench pictures was taken.

Table 1 shows the bench number, the date and time these data were taken, and the integrated neutron fluence the camera accumulated. Some data were taken at the same fluence. These were typically done at the beginning of the next day or at a new temperature.

b) Test Bench Pictures

The camera was aligned on the test bench and manually focused. The temperature of the cooler was recorded. Then the following set of pictures were taken (number in parentheses indicates number of pictures):

- (2) 1 msec exposure dark pictures (light source not triggered)
- (2) 1 msec exposure white pictures (light source triggered and no image slide installed)
- (2) 1 msec exposure image pictures (light source triggered and image slide installed)

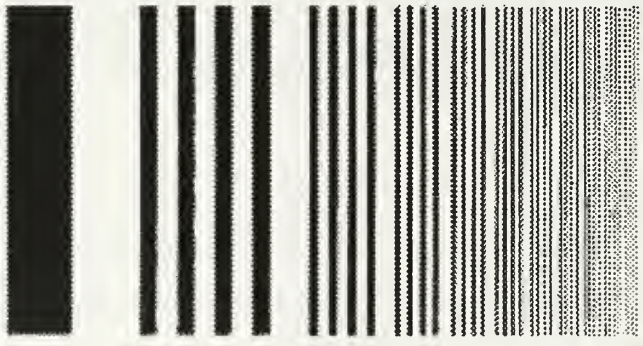

Figure 8. High resolution slide image

It was discovered after the 8th set of bench pictures that by taking 400 msec exposure pictures, the damage to the camera could be seen as slightly brighter pixels. This effect was not evident on the 1 msec exposure pictures so the picture set was modified to:

- 1 msec exposure dark pictures
- 400 msec exposure dark pictures
- 1 msec exposure white pictures
- 400 msec exposure white pictures

- 1 msec exposure image pictures
- 400 msec exposure image pictures

The camera was engineering grade with two vertical faults. These faults were at about 1/3 and 2/3 across the full 1152x1242-pixel picture. For this reason, all pictures were set to 400x1000-pixel pictures avoiding the two faults.

c) Temperature Control

The camera was cooled with a Peltier effect thermoelectric cooler via a closed looped proportional control circuit set at the controller. The experimental setup precluded use of vacuum in front of the CCD face, which was therefore at ambient pressure. The threat of condensation on the face of the camera and then possible shorting of the CCD head led us initially to run the experiment near room temperature.

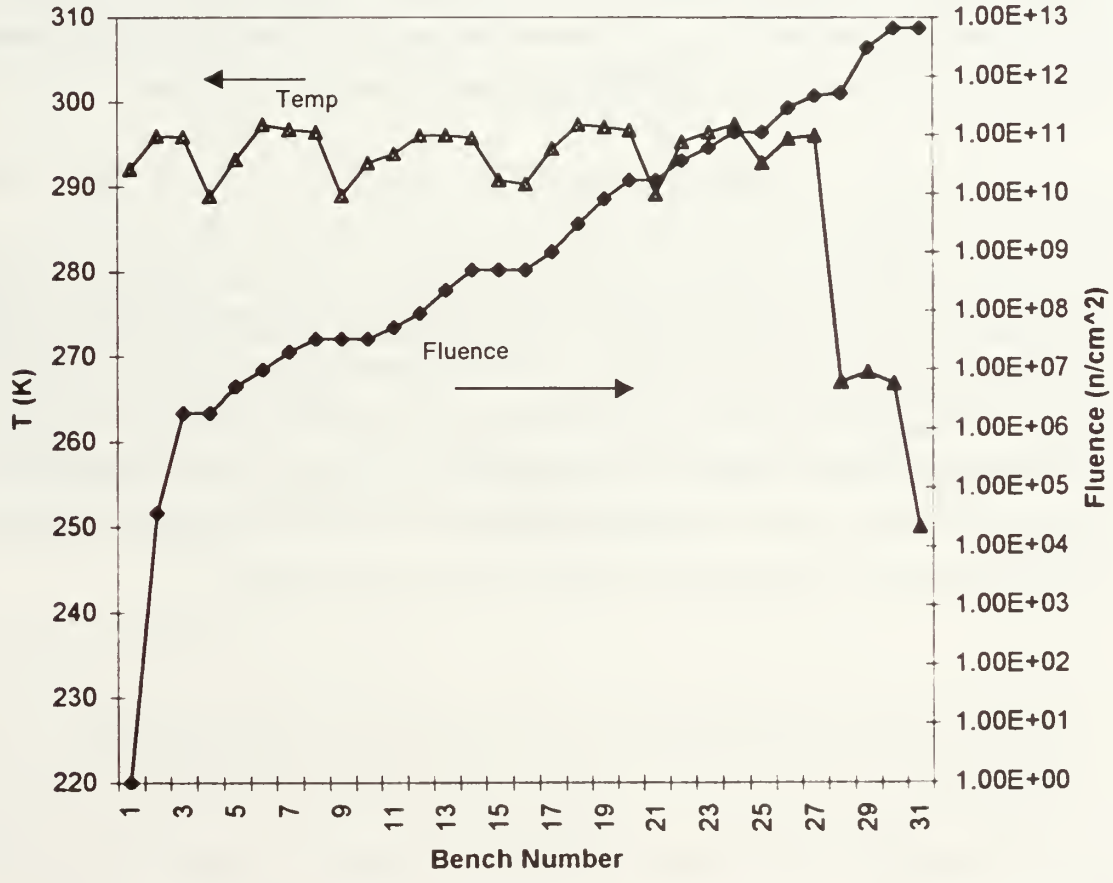

Figure 9. Temp and Fluence vs Bench Number, shows the camera's operating temperature for each measurement

For bench tests numbers 1 through 27 (see Table 1), the camera was operated without use of the Peltier cooler. The camera generates heat when energized. For these bench tests, heat was dissipated via the circulation of water by a small pump through its cooling jacket to a 2-gallon pail of water. This was not enough of a heat sink to maintain a constant temperature, and so the water and hence the camera slowly heated up through out a day's worth of irradiation and testing. At the end of each day, the camera was turned off and equilibrated to room temperature for the next day's use.

By the 27th bench test, the damage to the camera was extensive. The camera was operated at approximately 267 K to lower the dark current and was monitored for icing of the camera head. When possible, the face of the camera was sealed with tape to minimize icing. During camera transfers between the test bench and the radiation chamber, any icing was removed with a swab and alcohol.

Once again on the 30th bench test, extensive damage to the camera led to another lowering of temperature. This time the camera was lowered to 250 K, and the camera iced badly. No more irradiations were conducted. Only one image was taken for the last bench test, number 31. Figure 9 shows the measured camera face temperatures for each bench test and the corresponding integrated fluence is also graphed.

d) In Situation Pictures

While the camera was being irradiated, the camera was taking pictures, and these were saved to disk to visually monitor the performance of the camera. Illuminated and non-illuminated pictures were taken and are available for future analysis of transient effects. A telescope was used to illuminate the face of the CCD for the first 25 bench sets, after which, the camera's distance from the radiation source was too close to permit the telescope to fit and so only non-illuminated pictures were taken. Furthermore, the dark current had grown to the point that illuminated images were saturated.

IV. EXPERIMENTAL RESULTS

A. FLUENCE, GAIN, AND READOUT TIME

1. Gain

When the controller reads off the charge from each pixel, it converts the number of electrons read off into a digital value. To determine this conversion factor, called gain, counting statistics are utilized. Alan Conder at LLNL supplied this procedure by electronic mail correspondence. The average value, μ, of electrons, *e*, generated due to dark current in any cell is equal to the square of the standard deviation, σ. For a gain of g,

$$\mu(e) = g\mu(digital)$$

$$\sigma(e) = g\sigma(digital) = \sqrt{\mu(e)}$$

and solving for g yields:

$$g = \frac{\mu(digital)}{\sigma(digital)^2}$$

where digital is short for digital value of the pixel.

With two 1 msec pre-irradiated dark pictures, software was used to add 600 digital units to one picture and then to subtract the other picture from this modified picture. 600 units were used to preclude obtaining negative values, which would result in a digital zero. The standard deviation of the output of several 100-pixel-wide row segments was found from this new compound picture. Next, the average value for each of these same segments was found from an unaltered dark picture. Therefore for each segment, the average value of g was found: g = 5.2 e/digital count.

2. Fluence

The neutron activation threshold for Ni-57 is approximately 12 MeV. RTNS personnel correlated the deuteron current on target with neutron flux. A fluence, ϕ, of approximately 1.0×10^7 n/cm^2 is required to activate Ni-57 to levels readable with our equipment. Therefore, for the first 4 irradiations, deuteron current correlation was used to determine the fluence (see Table 1.) All subsequent fluence levels were determined from the activation results of Ni-57.

3. Readout Time

The time the controller takes to shift up and out the entire image is called the readout time, t_r. t_r was found by taking several pictures of different sizes and measuring the pulse duration of the readout trigger on an oscilloscope. By using the formula provided in the Princeton Instruments controller's manual:

$$t_r = XYt_1 + Yt_2$$

where X is the row size, Y is the column size, t_1 is the time required to shift a pixel out of the shift register and digitize it, and t_2 is the time to shift one row to the shift register, we obtained: $t_1 = 2$ μsec and $t_2 = 400$ μsec. This resulted in a readout time of $t_r = 1.23$ sec for the 400 x 1000 pixel picture used in this experiment.

B. DARK CURRENT

Dark current was explored with the dark pictures. By examining a 1 msec picture for every bench set, we are able to parameterize the results. Many of the unknown variables were determined using an iterative numerical process.

1. Digital Results Converted to Dark Current

a) Data Reduction to Rows

The dark pictures showed very good uniformity across the rows. For this reason and to simplify analysis, the dark pictures were reduced to the average value for each row. This provided us 1000 digital values for each picture. The average readout value of the row is R_j, where j is the row number from j = 1 to 1000.

Each pixel has an area, A, of 22.5 by 22.5 μm square. Multiplying the dark current by the area and the build-up time gives us the charge generated. Then, dividing by q to convert Coulombs to number of electrons and by g to convert number of electrons to a digital value, we obtain a digital result.

For the dark pictures, there are three contributors for the digital value in the pixels at read off. The first is dark current due to the exposure time plus set-up time, t_e. The second is dark current due to the readout time, t_r. The third is the bias value, b,

the controller assigns to the camera to preclude a zero being assigned for potential negative values.

$$R_j = \frac{A}{qg}(Jt_e + Jt_r \frac{j-1}{n-1}) + b \tag{8}$$

where n is the total number of rows. In this model, there is no build up of dark current in the first row due to read off.

Losses due to CTI are expressed in two ways. As each row of charge due to the exposure time is shifted up, only a fraction of charge, known as the Charge Transfer Efficiency ($c_e = 1 - \eta$), is transferred. This fractional loss occurs for each row shift and hence modifies the exposure term by the factor: $(c_e)^j$. The readout term is cumulative. As each row is shifted up, dark current generates charge, $AJ\frac{t_r}{n-1}$. However, this new charge suffers CTI losses as it shifts up as did the exposure term. The process of cumulative charge buildup, and subsequent degradation during shifts due to CTI losses, results in a series term: for the j[th] row, $\sum_{i=1}^{j-1} c_e^{\,i}$. This finite sum can be simplified to $\frac{c_e - (c_e)^j}{1 - c_e}$. Accounting for CTI in Equation 8 yields:

$$R_j = \frac{A}{qg}[Jt_e(c_e)^j + J\frac{t_r}{n-1}\frac{c_e - (c_e)^j}{1 - c_e}] + b \tag{9}$$

The data will now be used to find the unknown constants. For very low CTI, Equation 8 can be used to approximate the cell values. Differentiating Equation 8 with respect to j yields the slope of the row values:

$$\frac{d}{dj}R_j = \frac{A}{qg}J\frac{t_r}{n-1} \tag{10}$$

b) Temperature Function

Recall that J is modeled in Equation 7 as: $J = (J_0 + c\phi)f(T)$, where the temperature function, Equation 6, is expressed as: $f(T) = (T/T_0)^{3/2}e^{-E/kT}$. The value of E, in eV, was determined to be 0.635. Previously determined experimental values were 0.633 [Ref. 4] and 0.63 [Ref. 8]. The value of 0.635 was found by an iterative method.

Fully writing out Equation 8 gives us:

$$\frac{d}{dj}R_j = \frac{A}{qg}\frac{t_r}{n-1}(J_0 + c\phi)(T/T_0)^{3/2}e^{-E/kT}$$

The row slope is proportional to the temperature function for low CTI. The dominant term in the temperature function is the exponential one. Therefore, the log of the slope

should be nearly proportional to E/kT. The slope of the digital rows of each dark picture was measured for only 30 rows, to minimize CTI effects. Plotting the log of the slope versus 1/kT for low fluences yielded a line whose slope was –0.9. This was the entering argument for determining J_0 and c. As J_0 and c were determined (see sections c and d below), a wider range of fluences and temperatures (see Figure 1) were used to refine our final solution of E.

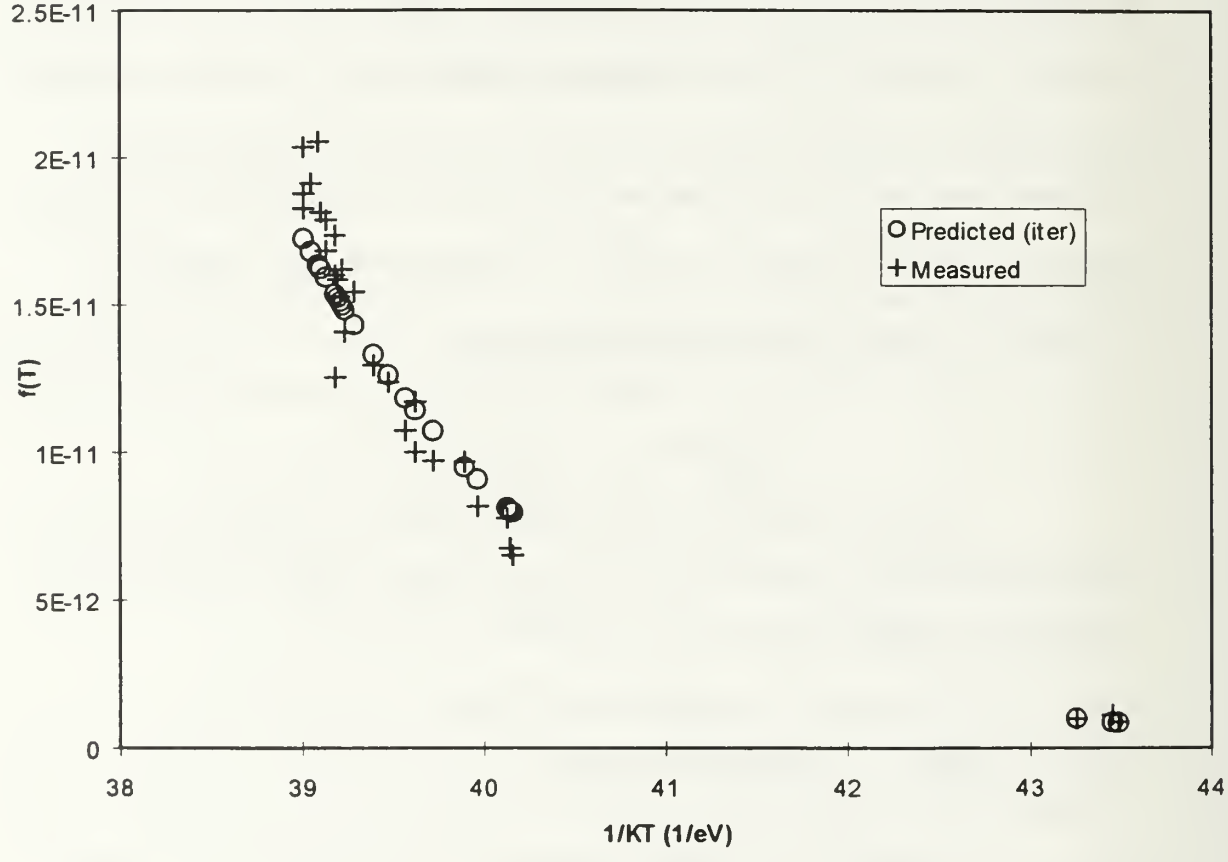

Figure 10. Measured and Predicted f(T)

We graphed in Figure 10 the values from our formula for f(T) (predicted) $f(T) = (T/T_0)^{3/2} e^{-E/kT}$ and the value for f(T) (measured). f(T) measured was obtained with the values of J_0 and c and the measured value of the slope: $f(T) = \frac{d}{dj} R_j \frac{qg}{A} \frac{n-1}{t_r} (J_0 + c\phi)^{-1}$. Furthermore, Figure 11 shows the deviation in E

required to match these values exactly.

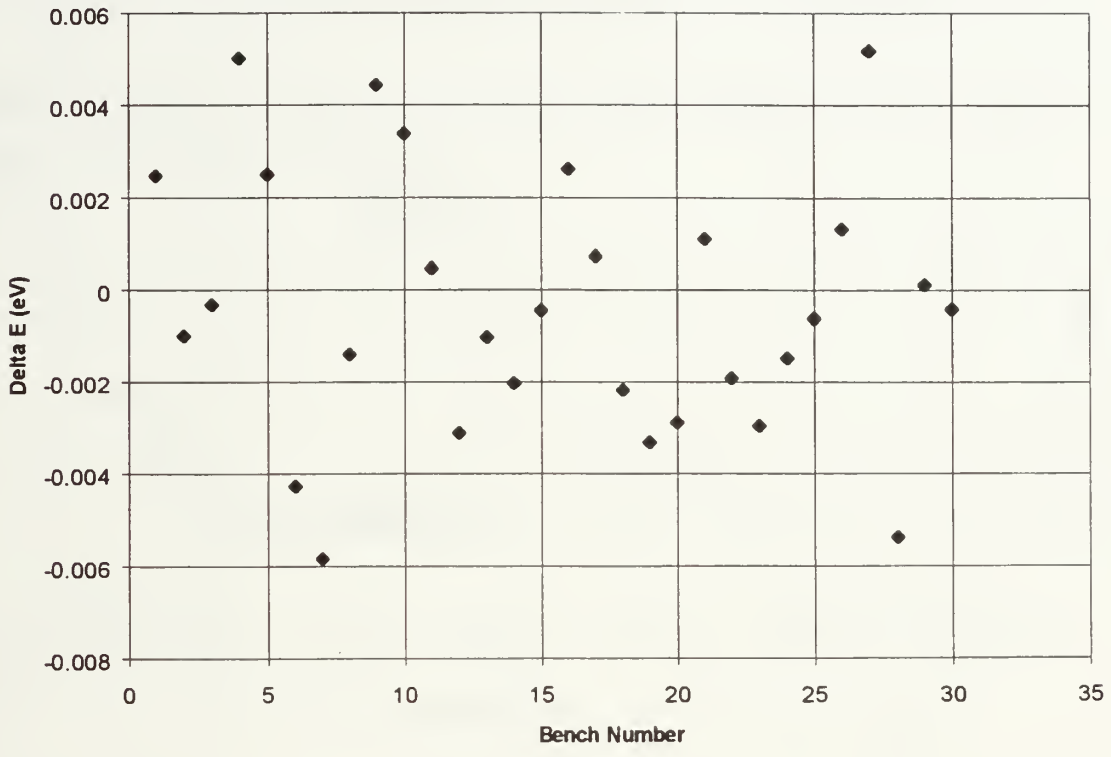

Figure 11. Delta E vs. Bench Number for E=0.635 eV with a standard deviation of $2.78x10^{-3}$ eV.

c) Temperature Independent Dark Current and Damage Coefficient

The temperature independent dark current, J_0, and damage coefficient, c, were found using Equation 10. Manipulation provides:

$$\frac{qg}{A}\frac{n-1}{t_r}\frac{1}{f(T)}\frac{d}{dj}R_j = \{\frac{J}{f(T)}\} = c\phi + J_0 \qquad (11)$$

With f(T) parameterized, Equation 11 is a linear equation having J_0 as an intercept and c as the slope. Due to the nearly 13 decade range of the fluence, a better fit for J_0 was found by averaging the value on the left side of Equation 11 for the first 12 bench pictures, where the fluence was small enough to ignore its contribution to J_0. The slope provided an excellent fit for c. The comparison of the measure and fitted values can be seen in Figure 12.

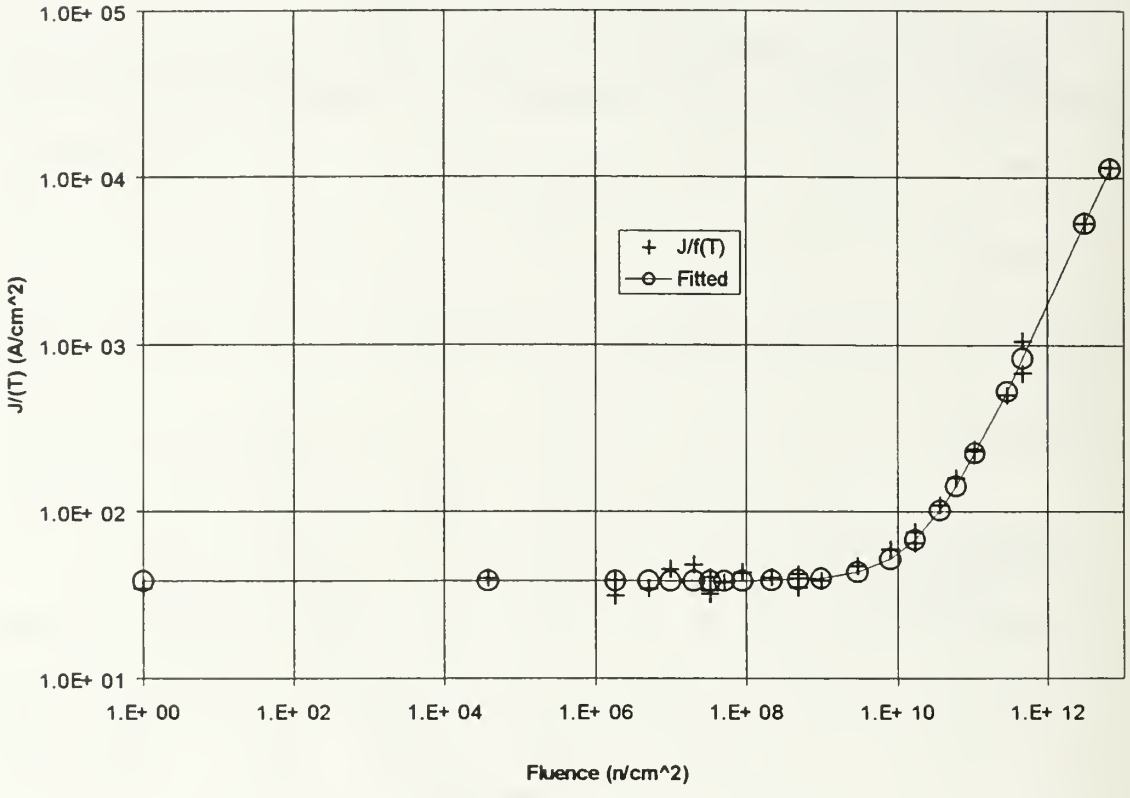

Figure 12. Fitted and Measured J/f(T) vs. Fluence

The value for the damage coefficient times the temperature function at 298 K agrees well with other experimental results as seen in Table 2[Ref. 8].

Table 2. Comparison of Damage Coefficient from Different Investigators

Reference	**c f(298) (nA/neutron)**	**Radiation Source**
Hartsell [Ref. 12]	~9.6 x 10^{-11}	Fast Burst Reactor (fission)
Saks [Ref.13]	1.9 x 10^{-10}	Cyclotron (0-30 MeV, peak 15 MeV)
Chang [Ref. 14]	~2 x 10^{-11}	Fast Burst Reactor (fission)
Srour [Ref. 8]	~4 x 10^{-11}	TRIGA reactor (fission)
Present work	3.1 x 10^{-11}	RTNS (fusion)

d) Exposure Time and Digital Bias

To solve for the exposure time and digital bias, we start with Equation 8: $R_j = \frac{A}{qg}(Jt_e + Jt_r \frac{j-1}{n-1}) + b$. By looking at the first row, j=1, this equation becomes linear: $R_1 = \frac{A}{qg} Jt_e + b$, with t_e as the slope and b as the intercept. The data can be seen in Figure 13 along with the fitted results.

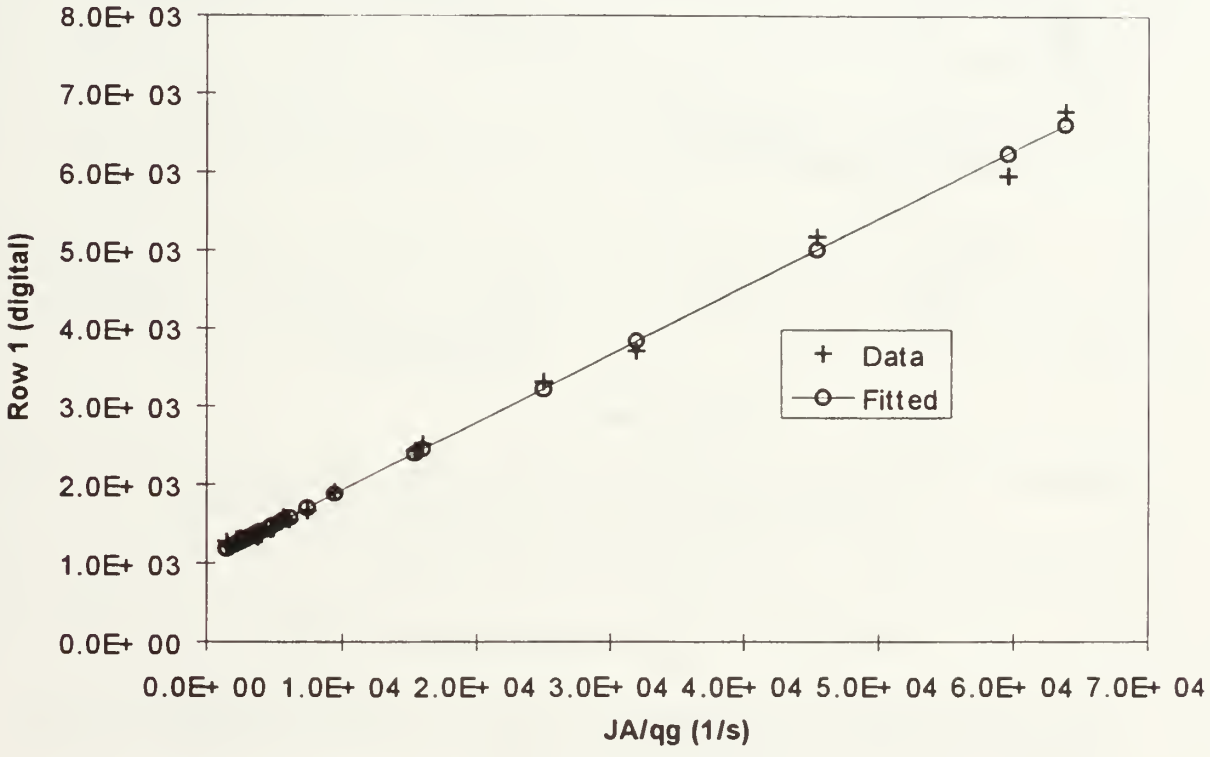

Figure 13. Exposure Time and Bias Determination

e) Charge Transfer Inefficiency

CTI effects are minimal for our previous considerations. However, CTI effects must be known to evaluate camera performance fully. Figure 14 shows how the

complete charge transfer, as seen in Equation 8: $R_j = \frac{A}{qg}(Jt_e + Jt_r \frac{j-1}{n-1}) + b$, compares with the raw data.

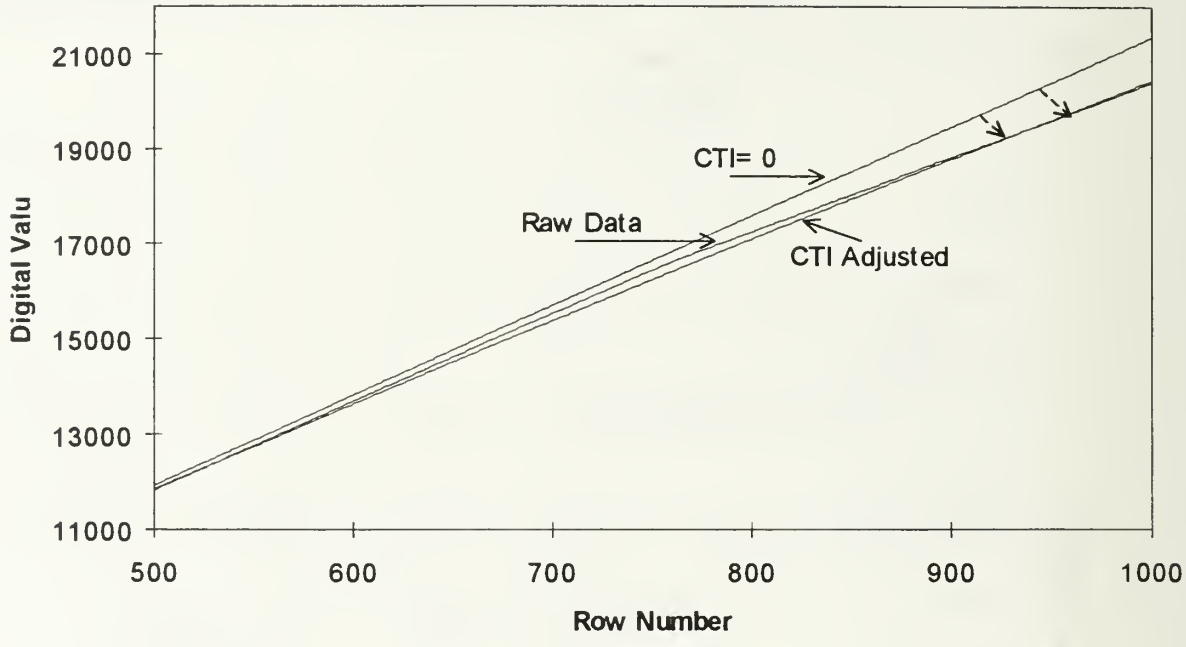

Figure 14. CTI Effects for Bench Number 11, The dashed arrows indicate how accounting for CTI lowers the slope and gives a close match between model and raw data.

Equation 9, $R_j = \frac{A}{qg}[Jt_e(c_e)^j + J\frac{t_r}{n-1}\frac{c_e-(c_e)^j}{1-c_e}] + b$, can be used to fit the raw data when CTI is not equal to zero. Figure 14 is plotted for the last 500 rows because CTI effects are not discernable for j<500.

Figure 15 shows how CTI changes for all the measurements as well as a linear trend line. This shows a linear dependence of CTI, η, over the fluence ϕ. From Equation 5:

$$\eta = \{qkTD_{it}/(Q_{sig} + Q_{bias})\}\ln(1 + Pn_z)$$

this result demonstrates a correlation between ϕ and the density of energy states, D_{it}.

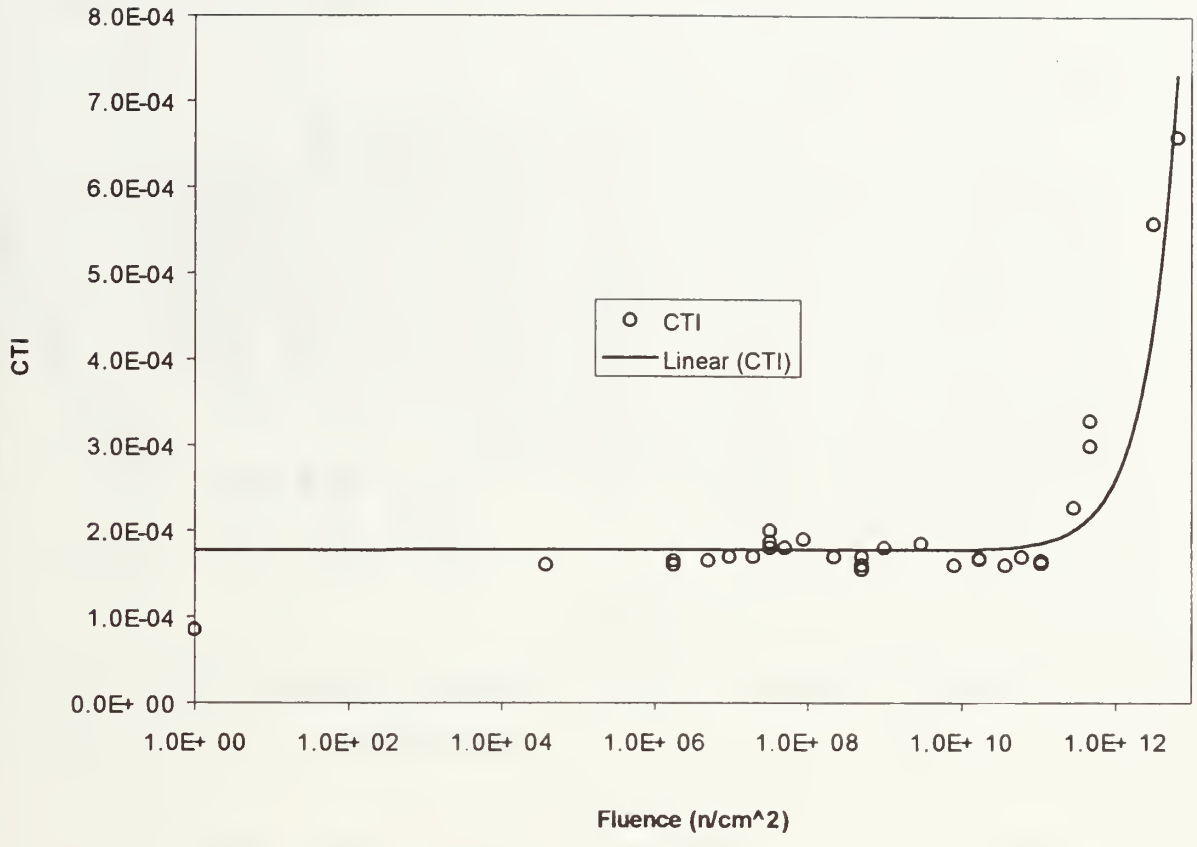

Figure 15. CTI vs. Fluence. This semilog plot shows a linear relation of CTI with fluence. The first data point is below the trendline, but unverifiable.

f) Dark Current End Results

The constants of the equation relating dark current to digital output

$$R_J = \frac{A}{qg}[Jt_e(c_e)^J + J\frac{t_r}{n-1}\frac{c_e-(c_e)^J}{1-c_e}] + b$$

has been solved. Considering a low CTI yields a good solution for the dark current: $J = \frac{qg}{A}\frac{n-1}{t_r}\frac{d}{dj}R_J$ from measurement of the slope. Comparison to the parameterized equation for dark current: $J = (J_0 + c\phi)f(T)$ can be seen in Figure 16. This shows good correlation between measured and fitted results over 13 decades of fluence and temperature ranges from 300 K to 267 K.

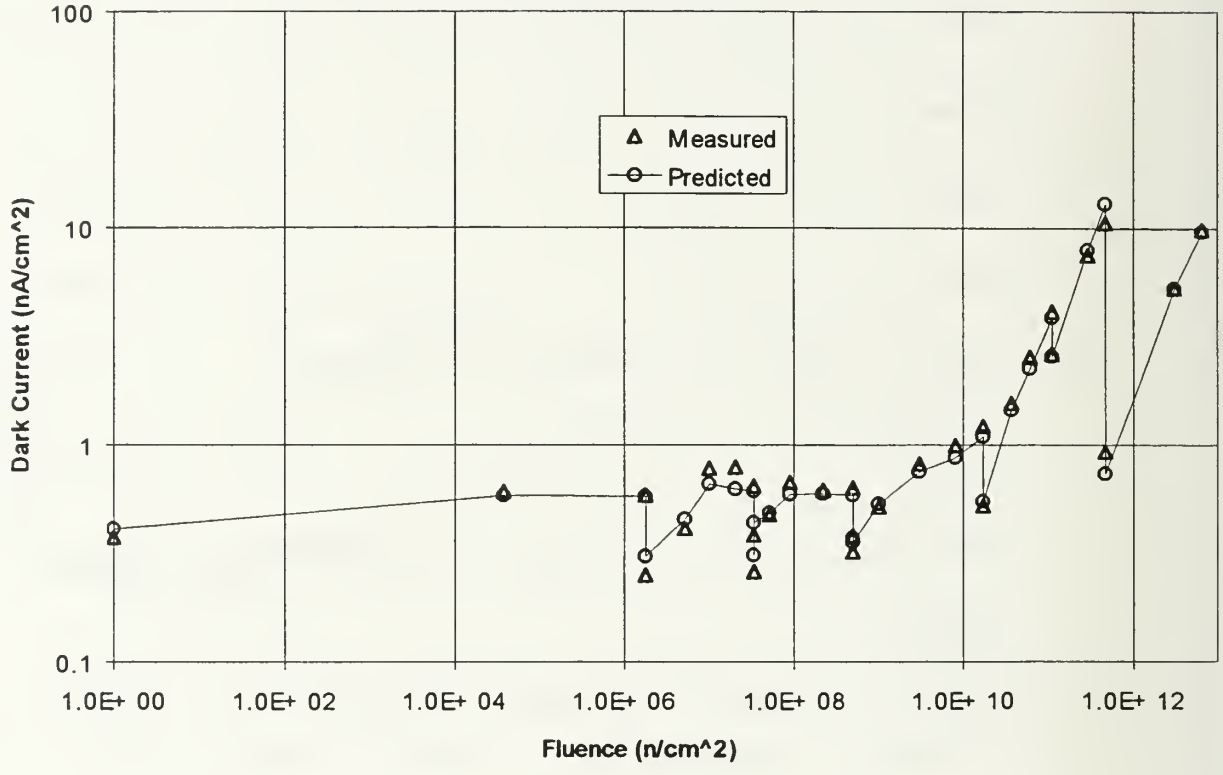

Figure 16. Dark Current, this chart compares the measured dark current to the fitted one.

C. CONTRAST TRANSFER FUNCTION

Contrast Transfer Function, CTF, is a measure of the resolution of square wave bar patterns. It is defined as: $CTF = \frac{L_{max} - L_{min}}{L_{max} - L_{min}}$, where L_{max} and L_{min} are the maximum and minimum digital values within a bar pattern [Ref. 10]. A perfect CTF would be 1.0

The pictures of the high-resolution images were of 10 sets of 4 bars and one set of one large bar. The bar sets image, as projected on the camera, varied in spatial frequency from about 1 pixel wide to about 30 pixels wide; see Figure 8. The average value of the columns versus column number is graphed in Figures 17 and 18.

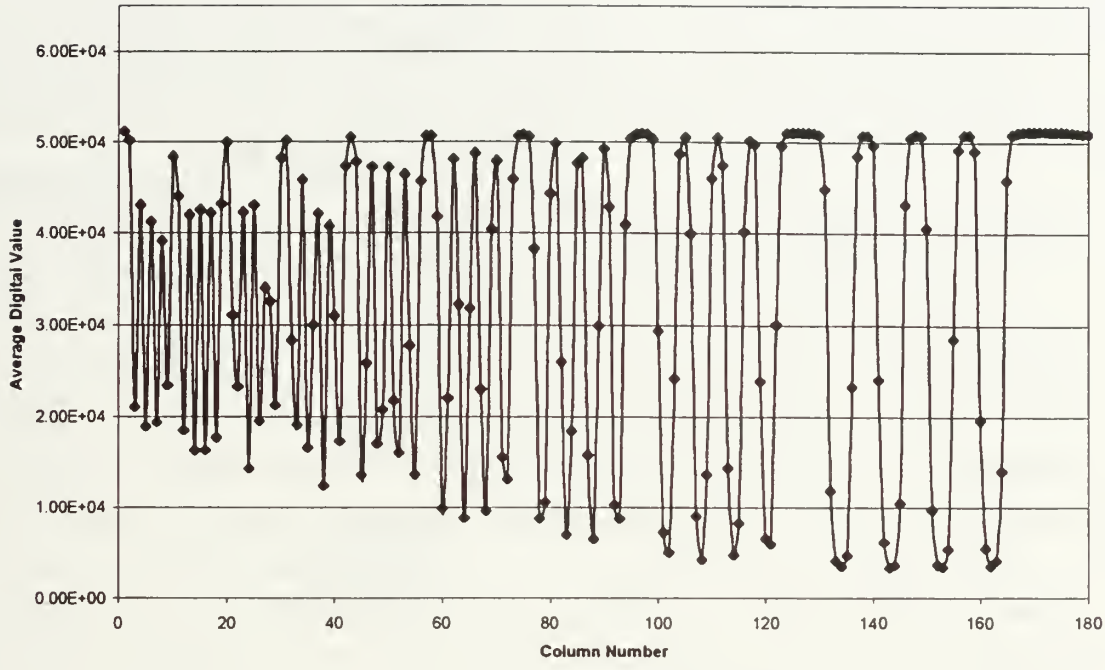

Figure 17. Partial Graph of Bar Pattern, a fit to the data points is shown.

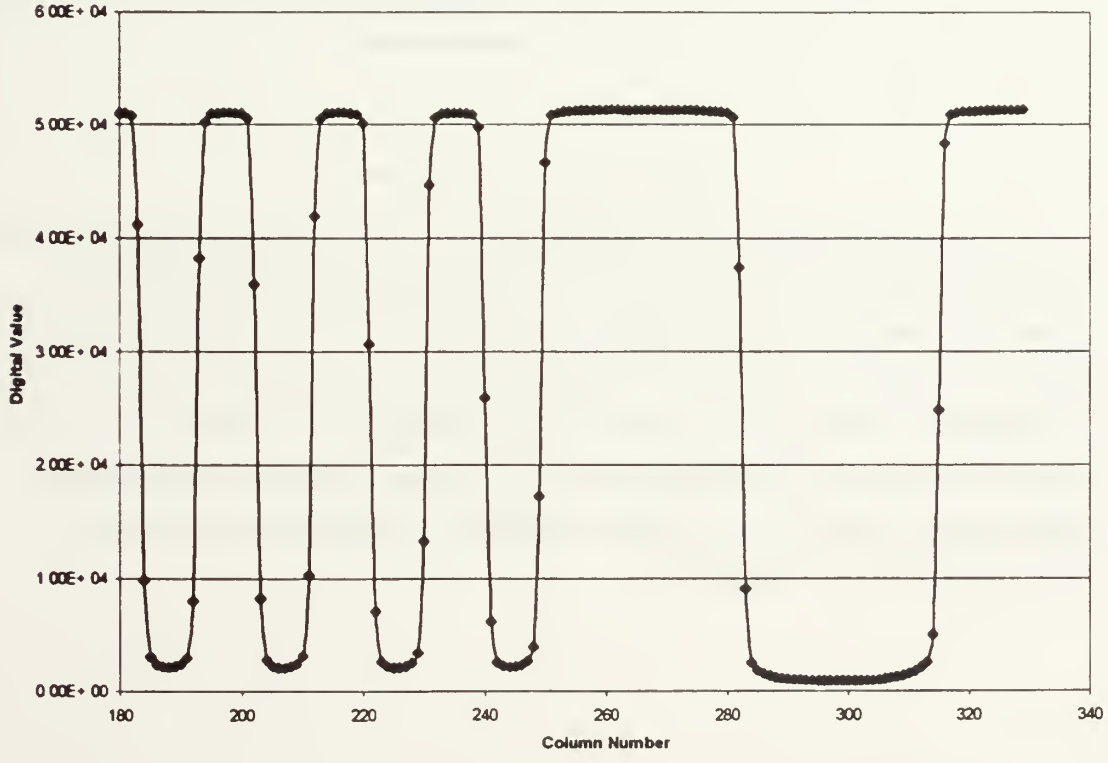

Figure 18. Continued Bar Graph

The digital value can be interpreted as bright for high and dark for a low value.

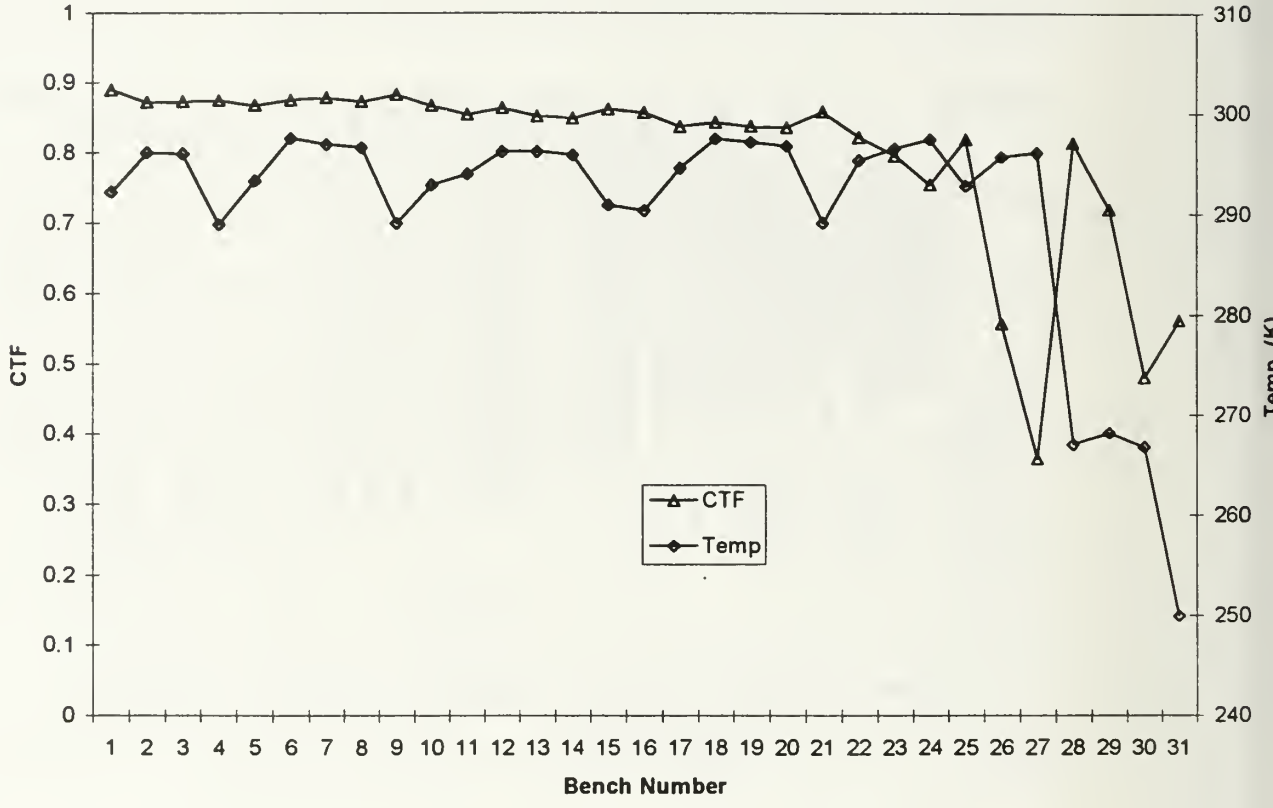

Figure 19. CTF and Temp. vs. Bench #

The CTF was calculated for each bar set for every bench test. A good measure of CTF performance is the 4 pixel wide bar set. Bar sizes smaller than this size were poor indicators because they were too close to the sampling size (1 pixel). Bars larger than this showed less degradation. Figure 19 shows that in general as the fluence increased, the CTF degraded. Two things caused lower CTF. With more dark current, there was more noise for the same signal. Furthermore, the CTI increased with fluence, which led to inefficient signal transfer. Lowering the temperature lowered the dark current and produced a partial recovery of CTF.

V. SUMMARY

This experiment shows that 14 MeV fusion neutron irradiation causes extensive damage to Charge Coupled Device (CCD) cameras. The damage mechanism is through atomic displacement of the atoms in the Complementary Metal Oxide Semiconductor (CMOS) pixels. Damaged pixels exhibit higher dark current and degraded charge transfer capabilities.

An accurate model of dark current is presented: $J = (J_0 + c\phi)f(T)$. This model accounts for variations due to accumulated fluence and temperature fluctuations. Temperature plays a dominant role in dark current. By lowering the temperature, there was is exponential drop in dark current, which partly compensates for the effects of irradiation. For a given temperature, the dark current increased linearly with fluence.

Charge Transfer Inefficiency (CTI) was examined with respect to fluence, and a linear increase was observed. Contrast Transfer Function (CTF), a ratio of the difference from maximum to minimum brightness of a bar image to the sum, was measured to investigate the effect of CTI and dark current on resolution. CTF degradation followed the trend of dark current. With increased dark current, there was more noise for the same amount of signal. Higher CTI also resulted in a lower signal because less signal properly transferred off the pixel to the controller.

APPENDIX CCD CAMERA SPECIFICATIONS

EEV 1152 x 1242 CCD Performance Characteristics as provided by Princeton Instruments

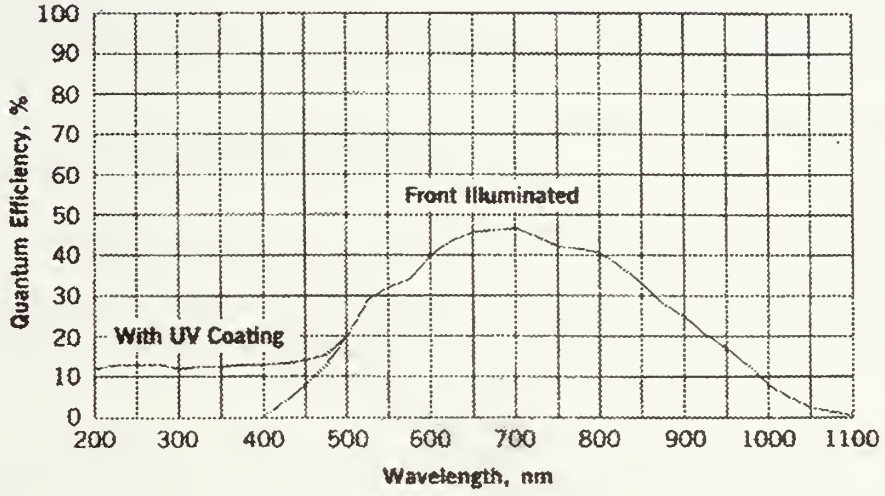

CCD Arrays:	EEV Model 05-30, standard
Format:	1152 x 1242 pixels
	25.9 x 27.5 mm overall,
	22.5 x 22.5 μm pixels
Full Well Capacity:	≥ 500,000 electrons
Readout Noise:	4-6 electrons at 50 kHz
	25 electrons at 1 MHz
Spectral Range:	400-1080 nm, see graph above
Dynamic Range:	16 bits
Response Nonlinearity:	1-2% for 16 bits
Response Nonuniformity:	≤ +/- 3% over entire CCD area
Scan Rate:	50 to 500 kHz

LIST OF REFERENCES

[Citation by number:]

1. Schroder, D. K., Modular Series on Solid State Devices, Advanced MOS Devices, Neudeck, G. W., Pierret, R. F., Ed. Addison-Wesley Publishing Company, Inc., 1987.

2. Boer, K. W., Survey of Semiconductor Physics, Electrons and Other Particles in Bulk Semiconductors, Van Nostrand Reinhold, 1990.

3. Kittel, C., Introduction to Solid State Physics, John Wiley and Sons, Inc., 1956.

4. Hopkinson, G. R., Dale, C. J., Marshall, P. W., *Proton Effects in Charge Coupled Devices*, pp. 614-627, IEEE Transactions on Nuclear Science, Vol. 43, No. 2, April 1996.

5. Srour, J. R., Hartmann, R. A., *Effects of Single Neutron Interactions in Silicon Integrated Circuits*, pp. 4195-4200, IEEE Transactions on Nuclear Science, Vol. NS-32, No. 6, December 1985 .

6. Pierret, R. F., Modular Series on Solid State Devices, Field Effect Devices, Addison-Wesley Publishing Company, Inc., 1990.

7. Belian, A. P., Morse, E. C., Tobin, M., Experimental 14-MeV Neutron Radiation Damage Assessment of Optical Materials for the National Ignition Facility Using RTNS-1, Berkeley Fusion Engineering, August 1996.

8. Srour, J. R., Chen, S. C., Othmer, S., Hartmann, R. A., *Neutron Damage Mechanisms in Charge Transfer Devices*, pp. 1251-1260, IEEE Transaction on Nuclear Science, Vol. NS-25, No. 6, December 1978.

9. Conder, A. D., Dunn, J., Young, B. K., *Miniature, Vacuum Compatible 1024x1024 Charge-Coupled Device Camera for X-ray, Ultraviolet, or Optical Imaging*, pp. 709-711, Review of Scientific Instruments, Vol. 66 (1), January 1995.

10. Pavan, P., Zanella, G., Zannoni, R., *Spatial Resolution in X-ray Imaging with Scintillating Glass Optical Fiber Plates*, pp. 600-604, Nuclear Instruments and Methods in Physics Research, A327, 1993.

11. Pierret, R. F., Modular Series on Solid State Devices, Volume IV, Field Effect Devices, Neudeck, G. W., Pierret, R. F., Ed. Addison-Wesley Publishing Company, Inc., 1990.
12. Harsell, G. A., *Proceedings of the 1975 International Conference on Applications of CCDs*, San Diego, CA, October 1975.

13. Saks, N. S., Killiany J. M., Baker, W. D., *Proceedings of NASA-JPL Conference on CCD Technology and Applications*, Washington D. C., December 1976.

14. Chang, C. P., Aubuchon, K. G., *Final Report on Contract N00173-76-C-0166*, March 1977.

INITIAL DISTRIBUTION LIST

1. Defense Technical Information Center 2
   8725 John J. Kingman Rd., STE 09944
   Ft. Belvoir, VA 22060-6218

2. Dudley Knox Library 2
   Naval Postgraduate School
   411 Dyer Rd.
   Monterey, CA 93943-5101

3. Lawrence Livermore National Laboratory 2
   Craig Sangster
   N-Division
   P.O. Box 808, L-481
   Livermore, CA 94550

4. William Maier 2
   PH/MW
   Naval Postgraduate School
   Monterey, CA 93943-5000

5. James Luscombe 1
   PH/LJ
   Naval Postgraduate School
   Monterey, CA 93943-5000

6. Xavier Maruyama 1
   PH/XK
   Naval Postgraduate School
   Monterey, CA 93943-5000

7. Don Walters 1
   PH/WE
   Naval Postgraduate School
   Monterey, CA 93943-5000

8. Christopher Amaden..... 4
   1205 Dockside Dr.
   Lutz, FL 33549